Characterization of MIMO antennas using spherical vector waves

Gustafsson, Mats; Nordebo, Sven

2005

CODEN:LUTEDX/(TEAT-7140)/1-9/(2005)

Characterization of MIMO antennas using spherical vector waves

Mats Gustafsson and Sven Nordebo

Department of Electroscience
Electromagnetic Theory
Lund Institute of Technology
Sweden

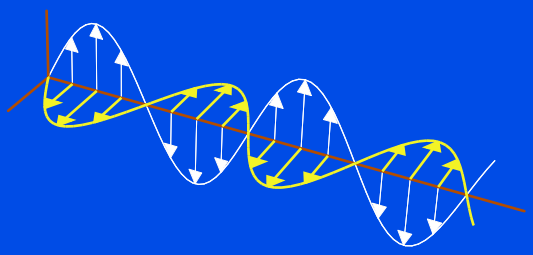

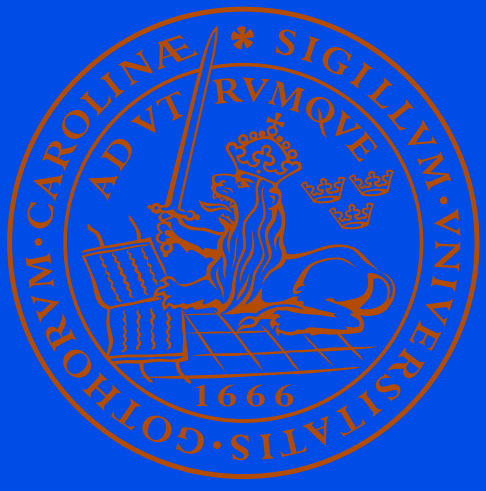

Mats Gustafsson
Mats.Gustafsson@es.lth.se

Department of Electroscience
Electromagnetic Theory
Lund Institute of Technology
P.O. Box 118
SE-221 00 Lund
Sweden

Sven Nordebo
Sven.Nordebo@msi.vxu.se

School of Mathematics and Systems Engineering
Växjö University
351 95 Växjö
Sweden

Editor: Gerhard Kristensson

Abstract

In this paper, spherical vector waves are used to analyze MIMO antennas. An expansion of the far-field pattern in spherical vector waves gives the correlation matrix and correlation loss of the MIMO antenna in uniform multi-path channels. Numerical examples of a MIMO tetrahedron and a MIMO cube are presented.

1 Introduction

Multiple-input multiple-output (MIMO) systems use multiple antennas at each end of the communication link in environments with rich multipath propagation. Recently, the MIMO systems have received much interest due to their ability to increase the spectral efficiency in wireless communication systems [5, 13, 15, 17, 18].

The tripole antenna is probably the simplest MIMO antenna. It consists of three orthogonal electric dipoles [1, 4]. To avoid the problem of feeding the dipoles at the same point in space and at the same time utilize the magnetic dipoles, a MIMO cube [6] or a MIMO tetrahedron can be used. These antennas consist of 12 and 6 electrical dipoles centered on the edges of a cube and a tetrahedron, respectively.

In this paper, spherical vector waves are used to analyze MIMO antennas. A mode expansion of the far field gives a natural expression of the polarization, angle, and spatial diversity that is utilized in MIMO systems [5, 7, 15, 17, 18]. This map gives a correlation matrix of the antenna in uniform multi-path environments and it offers a simple interpretation of the antenna radiation properties. Although this mode expansion is infinite, it is in practice sufficient to consider a finite set of modes due to the high Q-factors (strong reactive near field), and hence high losses and low bandwidth, associated with high order modes [7–10].

2 Antenna scattering matrix

We consider an antenna system with N local ports with incoming waves $\boldsymbol{v}$ and outgoing waves $\boldsymbol{w}$. The incoming and outgoing waves are power normalized, *i.e.*, the power in the incoming and outgoing waves are $\|\boldsymbol{v}\|^2 = \sum_n^N |v_n|^2$ and $\|\boldsymbol{w}\|^2$, respectively. The electromagnetic field is expanded in incoming, $\mathbf{u}_\alpha^{(3)}$, and outgoing, $\mathbf{u}_\alpha^{(4)}$, spherical vector waves [8] or modes

$$\boldsymbol{E}(\boldsymbol{r}) = k\sqrt{2\eta}\sum_\alpha a_\alpha\, \mathbf{u}_\alpha^{(3)}(k\boldsymbol{r}) + b_\alpha\, \mathbf{u}_\alpha^{(4)}(k\boldsymbol{r}), \tag{2.1}$$

where $\boldsymbol{r}$ is the spatial coordinate, k the wavenumber, and η the impedance, see appendix. This expansion is valid in the region outside a sphere surrounding the antenna. We use a power normalization of the expansion coefficients such that the power of the incoming and the outgoing waves are $\|\boldsymbol{a}\|^2 = \sum_\alpha |a_\alpha|^2$ and $\|\boldsymbol{b}\|^2$, respectively. The multi index $\alpha = \{\tau, s, m, l\}$ for $l = 1, 2, \ldots$, $s = 1, 2$, $m = 0, 1, \ldots, l$, and $\tau = 1, 2$ is introduced to simplify the notation. The index, α, is also ordered such that $\alpha = 2(l^2 + l - 1 + (-1)^s m) + \tau$.

There are a few common versions of the spherical vector waves in the literature [2, 3, 8, 10, 11]. Here, we follow [3, 10] and use $\cos m\phi$ and $\sin m\phi$ as basis functions in the azimuthal coordinate. This choice is motivated by the interpretation of the field related to the first 6 modes as the field from different elementary dipoles. The modes labeled by $\tau = 1$ (odd α) identify magnetic 2^l-poles and the terms labeled by $\tau = 2$ (even α) correspond to electric 2^l-poles. Moreover, the dipoles corresponding to $\alpha = 1, 2$ are directed in the y-direction, $\alpha = 3, 4$ in the z-direction, and $\alpha = 5, 6$ in the x-direction.

The scattering matrix of an antenna relates the incoming waves with the outgoing waves [8]. The antenna scattering matrix is

$$\begin{pmatrix} \mathbf{\Gamma} & \mathbf{R} \\ \mathbf{T} & \mathbf{S} \end{pmatrix} \begin{pmatrix} \boldsymbol{v} \\ \boldsymbol{a} \end{pmatrix} = \begin{pmatrix} \boldsymbol{w} \\ \boldsymbol{b} \end{pmatrix}, \tag{2.2}$$

where $\mathbf{\Gamma}$ is an $N \times N$ matrix, $\mathbf{R}$ is an $N \times \infty$ matrix with elements $R_{n,\alpha}$, $\mathbf{T}$ is an $\infty \times N$ matrix with elements $T_{\alpha,n}$, and $\mathbf{S}$ is an $\infty \times \infty$ matrix. The transmission matrix, $\mathbf{T}$, is determined by a projection of the far field on the spherical vector harmonics, $\mathbf{A}_\alpha$, *i.e.*, the far field of port n is

$$\boldsymbol{F}_n(\hat{\boldsymbol{r}}) = k\sqrt{2\eta} \sum_\alpha \mathrm{i}^{l+2-\tau} T_{\alpha,n}\, \mathbf{A}_\alpha(\hat{\boldsymbol{r}}) v_n, \tag{2.3}$$

where $\mathbf{A}_\alpha$ is defined in (A.2) and $\hat{\boldsymbol{r}} = \boldsymbol{r}/|\boldsymbol{r}|$. The Lorentz reciprocity theorem [8] gives $R_{n,\alpha} = (-1)^s T_{\alpha,n}$ for reciprocal antennas.

The receiving antenna is characterized by $\boldsymbol{v} = \mathbf{0}$ giving the received signal $\boldsymbol{w} = \mathbf{R}\boldsymbol{a}$. This can be interpreted as a receiving antenna channel, *i.e.*, it maps the incoming spherical vector waves, $\boldsymbol{a}$, to the received signals, $\boldsymbol{w}$. The power of the incoming wave is $\|\boldsymbol{a}\|^2$ and the received power is $\|\boldsymbol{w}\|^2 \leq \|\boldsymbol{a}\|^2$ as the antenna is passive. The properties of the channel is analyzed with a singular value decomposition (SVD) of the channel matrix $\mathbf{R} = \mathbf{U}\mathbf{\Sigma}\mathbf{V}^{\mathrm{H}}$, giving

$$\tilde{\boldsymbol{w}} = \mathbf{U}^{\mathrm{H}}\boldsymbol{w} = \mathbf{\Sigma}\mathbf{V}^{\mathrm{H}}\boldsymbol{a} = \mathbf{\Sigma}\tilde{\boldsymbol{a}}, \tag{2.4}$$

where $\mathbf{\Sigma}$ has at most N non-zero singular values σ_n.

3 Rayleigh channel

The Rayleigh channel is defined as a channel with uncorrelated and zero mean entries having complex Gaussian distribution and the amplitudes thus being Rayleigh distributed [14–16, 18], *i.e.*, $\mathbf{H} = \mathbf{H}_{\mathrm{w}}$, where $\mathcal{E}\{\mathbf{H}_{\mathrm{w}}\} = 0$ and $\mathcal{E}\{\mathbf{H}_{\mathrm{w}}|_{ij}\mathbf{H}_{\mathrm{w}}^*|_{mn}\} = \delta_{im}\delta_{jn}$. It is customary to interpret the scalar Rayleigh channel as the channel resulting from a large number of independent and uniformly distributed scattered waves impinging on the receiver [12]. Similar arguments show that a large number of uniformly distributed and independent scattered plane wave components impinging on an antenna can be represented as a Rayleigh channel in the spherical vector waves [7].

In this paper, we consider the limitations imposed by the antenna in uniform multi-path environments. The multi-path environment is modeled with a Rayleigh

channel $\mathbf{H}_{\mathrm{w}}$, giving the random channel $\mathbf{R}\mathbf{H}_{\mathrm{w}}$. It is observed that $\mathbf{R}$ can be interpreted as the square root of the correlation matrix on the receiver side [15]. We assume that the transmitter side consists of N_{s} uncorrelated ports with signals $\boldsymbol{s}$. The received signal is corrupted with noise, $\boldsymbol{y} = \mathbf{R}\mathbf{H}_{\mathrm{w}}\boldsymbol{s} + \boldsymbol{n}$, where the noise is assumed to be uncorrelated complex Gaussian noise [14, 15, 18] with spectral density N_0. The SVD of $\mathbf{R}$ in (2.4) gives the equivalent channel

$$\tilde{\boldsymbol{y}} = \boldsymbol{\Sigma}\widetilde{\mathbf{H}}_{\mathrm{w}}\boldsymbol{s} + \tilde{\boldsymbol{n}}, \tag{3.1}$$

where $\boldsymbol{\Sigma}$ and $\widetilde{\mathbf{H}}_{\mathrm{w}}$ are a diagonal $N \times N$ matrix with elements σ_n and an $N \times N_{\mathrm{s}}$ Rayleigh channel, respectively. The ergodic capacity (in $\mathrm{b\,s^{-1}Hz^{-1}}$) of this channel is given by

$$\overline{C}_{\boldsymbol{\Sigma}} = \mathcal{E}\left\{ \max_{\mathrm{Tr}\,\mathbf{R}_{ss}=N_{\mathrm{s}}} \log_2 \det\left(\mathbf{I} + \frac{P}{N_0 N_{\mathrm{s}}} \boldsymbol{\Sigma}\widetilde{\mathbf{H}}_{\mathrm{w}}\mathbf{R}_{\mathrm{ss}}\widetilde{\mathbf{H}}_{\mathrm{w}}^{\mathrm{H}}\boldsymbol{\Sigma} \right) \right\}, \tag{3.2}$$

where $\mathbf{R}_{\mathrm{ss}}$ is the power normalized covariance matrix for the input signal [15], $\mathbf{I}$ is the $N \times N$ identity matrix, and P/N_0 represents the signal-to-noise ratio. The optimal energy allocation is given by the water-filling solution [15]. The correlation loss (assuming $= 0\boldsymbol{\Gamma} = 0$) of the antenna channel, $\boldsymbol{\Sigma}$, is given by

$$\Delta C = \overline{C}_{\boldsymbol{\Sigma}} - \overline{C}_{\boldsymbol{\Sigma}=\mathbf{I}}. \tag{3.3}$$

The correlation loss [15] at high SNR, *i.e.*, neglect the identity matrix, $\mathbf{I}$, in (3.2), of this channel is given by

$$\Delta C_\infty = \log_2 \det(\boldsymbol{\Sigma}^2) = \sum_{n=1}^{N} \log_2 \sigma_n^2. \tag{3.4}$$

4 Numerical examples

4.1 MIMO tetrahedron

The MIMO tetrahedron consists of six electric dipoles centered on the edges of a tetrahedron (see Fig. 1a). This gives a maximum of six ports for the antenna, *i.e.*, $N = 6$. The antenna channel $\mathbf{T}$ is determined by a projection of the far-field patterns of each dipole on the spherical vector harmonics. The antenna is assumed be matched ($\boldsymbol{\Gamma} = \mathbf{0}$) at the considered frequency and to conserve power. This gives a total channel gain $\|\mathbf{T}\|_{\mathrm{F}}^2 = \sum \sigma_n^2 = 6$. For a mismatched antenna ($\boldsymbol{\Gamma} \neq \mathbf{0}$), the total channel gain is less than 6. In Fig. 1b, the mode representation of the MIMO tetrahedron contained in a sphere with radius of 0.3 wavelengths is depicted. The figure contains 6 graphs, where graph number n contains the amplitudes of the column number n of $\mathbf{T}$, *i.e.*, the far field of dipole number n (see Fig. 1a). The amplitude of bar indexed α corresponds to the magnitude of the α-th mode. As seen by the mode representation, both electric dipoles (α even) and magnetic dipoles (α odd) are included in the representation. It is also observed that each

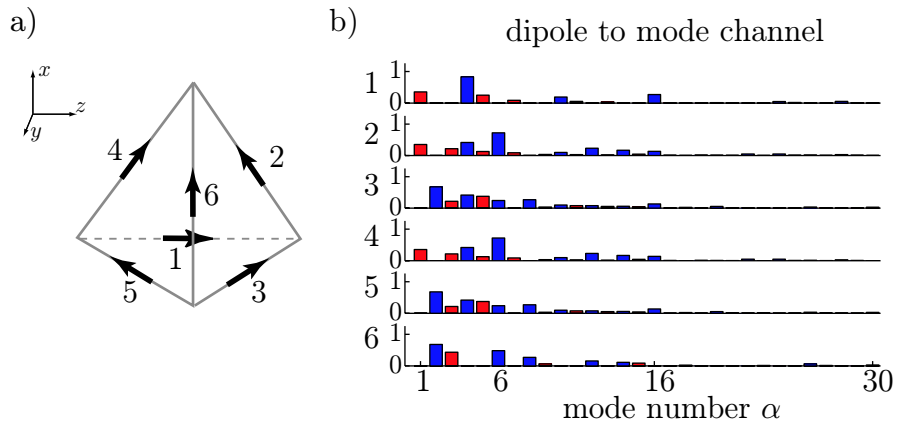

Figure 1: a) MIMO tetrahedron. b) Mode representation of each dipole on a MIMO tetrahedron with size 0.3λ, *i.e.*, each graph represents one column of $\mathbf{T}$ and the mode numbers represent the rows of $\mathbf{T}$.

dipole excites several modes and that the amplitude decreases for large values of the l index. Observe that $l = 1$ and $l = 2$ correspond to $1 \leq \alpha \leq 6$ and $7 \leq \alpha \leq 16$, respectively.

The singular value decomposition (2.4) is used to rewrite the antenna channel into a sum of orthogonal channels. In Fig. 2a, the 6 orthogonal channels, *i.e.*, the columns of $\mathbf{\Sigma U}^{\mathrm{H}}$, are depicted. Each graph shows one column and they are ordered from top to bottom. It is observed that the first three singular values σ_i, $i = 1, 2, 3$ correspond to three orthogonal dipoles plus a small contribution from higher order modes. The next three singular values σ_i, $i = 4, 5, 6$ correspond to the three orthogonal magnetic dipoles plus a small contribution from higher order modes.

In Fig. 2b, the magnitude of the singular values are plotted in decibel as a function of the size of the tetrahedron. Here, it is seen that the electric dipoles dominate the radiated field if the tetrahedron is small, *e.g.*, smaller than 0.3 wavelengths. As the size of the tetrahedron increases the influence of the magnetic dipoles and higher order modes increases. For a size of 0.5 wavelengths the contribution from the electric dipoles and the magnetic dipoles are of the same magnitude. Observe, that there are only two different singular values, *i.e.*, $\sigma_1 = \sigma_2 = \sigma_3$ and $\sigma_4 = \sigma_5 = \sigma_6$.

In Fig. 3a, the ergodic capacity, given by (3.2), for $N_{\mathrm{s}} = 6$ and the SNR values of $100, 10, 1$, and 0.1 is compared between the MIMO tetrahedron, $\overline{C}_{\mathbf{\Sigma}}$, (solid lines), the uncorrelated cases (dotted lines), $\overline{C}_{\mathbf{I}}$, and the high SNR approximation, $\overline{C}_{\mathbf{I}} + \Delta$ (dashed lines). The ergodic capacity is determined with the water-filling solution [15] over 1000 realization. The ergodic capacity increases up to its maximum at $r \approx \lambda/2$, *i.e.*, where the antenna channel is uncorrelated ($\mathbf{\Sigma} = \mathbf{I}$).

The limitations imposed by the antenna is better illustrated with the correlation loss (3.3), *i.e.*, the difference between the solid and dotted lines in Fig. 3a. The correlation loss is shown by the solid curves in Fig. 3b. The correlation loss is negligible for small SNRs where the spatial diversity is not utilized. The correlation loss increases up to the asymptotic value (3.4) for higher SNRs. The singular values,

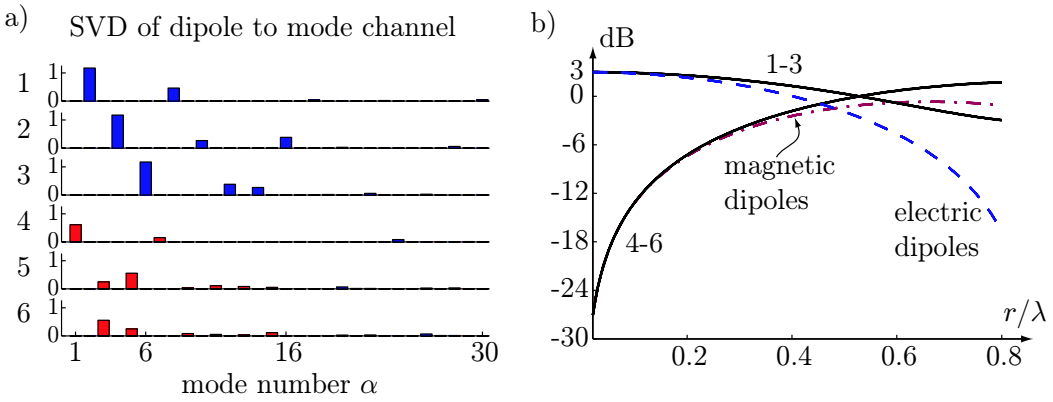

Figure 2: Characteristics of the MIMO tetrahedron after a SVD. a) The mode representation of the orthogonal channels *i.e.*, the columns and rows of $\mathbf{\Sigma U}^{\mathrm{H}}$. The channels are dominated by electrical dipoles (even numbers) and magnetic dipoles (odd numbers), respectively. b) the solid lines show the singular value distribution, *i.e.*, the channel gain, as a function of the tetrahedron size where each line correspond to three singular values. The dashed and dashed dotted lines show the projection on electric ($\alpha = 2, 4, 6$) and magnetic ($\alpha = 1, 3, 5$) dipoles, respectively.

σ_i^2, from Fig. 3b are redrawn in $\log_2$ scale in the figure to clarify their relation to the correlation loss (3.4). The $\log_2$ scale is used for a direct comparison with the loss in ergodic capacity given in $\mathrm{b\,s^{-1}Hz^{-1}}$. Observe that $10\log_{10}\sigma_i^2 \approx 3\log_2\sigma_i^2$. The corresponding average number of used channels are shown in Fig. 3c.

4.2 MIMO cube

The MIMO cube consists of 12 electric dipoles centered on the edges of a cube, see Fig. 4a. It is easily understood that the antenna channel of a small MIMO cube is dominated by the three orthogonal electric dipoles as four closely spaced dipoles oriented in the same direction are indistinguishable. This is also observed in Fig. 4b where the gain of each orthogonal channel is plotted as a function of the radius of the smallest sphere containing the antenna. In the figure, it is seen that a small cube is dominated by first three channels. The radiation patterns of these first three channels correspond to the radiation pattern of three orthogonal dipoles. As the sphere radius increases the contribution from magnetic dipoles and higher order modes increases and at $r \approx \lambda/2$, there are 12 orthogonal modes of almost equal gain.

The ergodic capacity, the correlation loss, and the average number of used channels are shown in Fig. 5 for $N_{\mathrm{s}} = 12$. It is seen that the MIMO cube has an average of approximately 11 independent channels for an SNR of 100 if the cube is close to $\lambda/2$, *cf.*, [6]. The results are similar as for the tetrahedron. The ergodic capacity of the cube is approximately two times the capacity of the tetrahedron for the approximately uncorrelated cases, $\mathbf{\Sigma} \approx \mathbf{I}$. However, the correlation loss is much higher for the cube than the tetrahedron for small antennas. This is easily understood by the

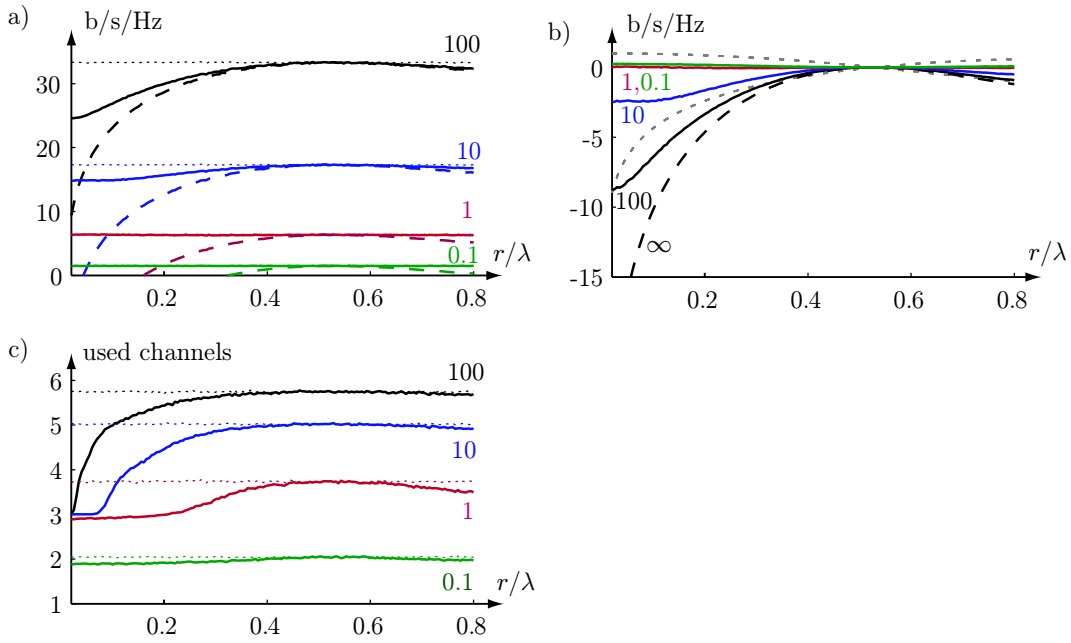

Figure 3: Properties of the MIMO tetrahedron as a function of the antenna radius for SNR values of $100, 10, 1$, and 0.1. a) The ergodic capacity. The solid and dotted lines show the ergodic capacity using (3.2) for the MIMO tetrahedron, $\overline{C}_{\mathbf{\Sigma}}$, and the uncorrelated case, $\overline{C}_{\mathbf{I}}$, respectively. The dashed lines show the ergodic capacity in the high SNR approximation, $\overline{C}_{\mathbf{I}} + \Delta C$, using (3.4). b) The solid lines show the correlation loss, (3.3), for the SNR values above. The dashed line shows the high SNR case (3.4). The channel gain from Fig. 2b are shown in $\log_2$ scale by the dotted lines. c) Comparison between the average number of used channels of the MIMO tetrahedron case (solid lines) and the uncorrelated case (dotted lines).

distribution of the singular values and physically understood from the difficulty to generate higher order modes in small antennas.

5 Discussion and conclusions

In this paper, spherical vector waves are used to analyze MIMO antennas. The correlation matrix of the antenna is obtained from the mode expansion of the far field. A singular value decomposition of the correlation matrix gives an equivalent representation of the antenna in terms of electric and magnetic 2^l poles. For future research, we will consider more realistic channel models and improve the models of the MIMO antenna by including mutual coupling between the antenna ports and by considering a realistic feed model.

Acknowledgments

The financial support by the Swedish research council is gratefully acknowledged.

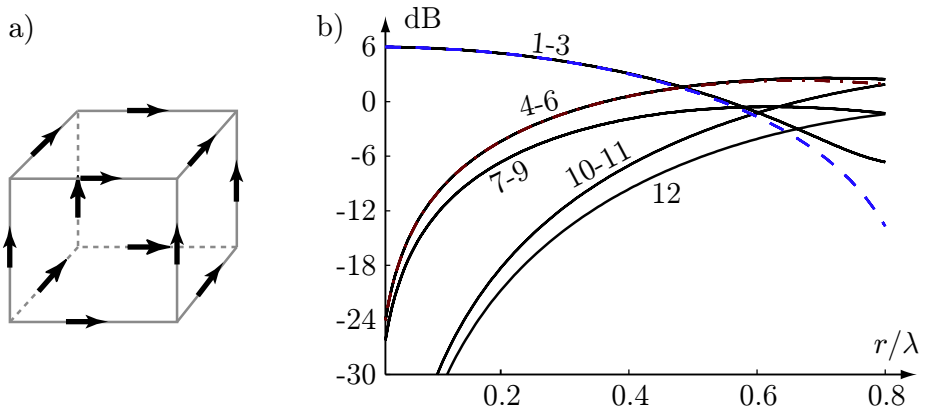

Figure 4: a) a MIMO cube, *i.e.*, a cube with an electrical dipole on each edge. b) the singular value distribution. The dashed and dashed dotted lines show the projection on electric and magnetic dipoles, respectively.

Appendix A Spherical vector waves

The incoming, $\mathbf{u}_\alpha^{(3)}$, and outgoing, $\mathbf{u}_\alpha^{(4)}$, spherical vector waves are given by

$$\mathbf{u}_{1sml}^{(p)}(k\boldsymbol{r}) = \mathrm{h}_l^{(p-2)}(kr)\,\mathbf{A}_{1sml}(\hat{\boldsymbol{r}}) \tag{A.1}$$

and $\mathbf{u}_{2sml}^{(p)} = k^{-1}\nabla \times \mathbf{u}_{1sml}^{(p)}$ where $\mathrm{h}_l^{(p-2)}, p = 3, 4$ denote the spherical Hankel functions, $\mathbf{A}_\alpha$ denote the spherical vector harmonics, $r = |\boldsymbol{r}|$, and time convention $\mathrm{e}^{\mathrm{i}\omega t}$ is used. The cases $p = 1, 2$ are used to denote standing spherical vector waves [8]. There are several common definitions of the spherical vector harmonics [2, 3, 8, 11]. For $\tau = 1, 2$, we use

$$\mathbf{A}_{1sml}(\hat{\boldsymbol{r}}) = \frac{1}{\sqrt{l(l+1)}}\nabla \times (\boldsymbol{r}\,\mathrm{Y}_{sml}(\hat{\boldsymbol{r}})) \tag{A.2}$$

and $\mathbf{A}_{2sml}(\hat{\boldsymbol{r}}) = \hat{\boldsymbol{r}} \times \mathbf{A}_{1sml}(\hat{\boldsymbol{r}})$ where Y_{sml} denotes the spherical harmonics [3]. The spherical vector waves (A.1) are trivially related to the spherical vector waves defined in [8] through

$$\mathbf{u}_{\tau,s,m,l}^{(p)} = \frac{\mathbf{F}_{\tau,m,l}^{(p)} + (-1)^{m+s}\mathbf{F}_{\tau,-m,l}^{(p)}}{-\sqrt{2}(-\mathrm{i})^s} \tag{A.3}$$

and $\mathbf{u}_{\tau,2,0,l}^{(p)} = \mathbf{F}_{\tau,0,l}^{(p)}$. Observe that $m \geq 1$ for $s = 1$ and that $s = 1$ and $s = 2$ correspond to odd, o, and even, e, modes, respectively.

References

[1] M. R. Andrews, P. P. Mitra, and R. de Carvalho. Tripling the capacity of wireless communications using electromagnetic polarization. *Nature*, **409**, 316–318, January 2001.

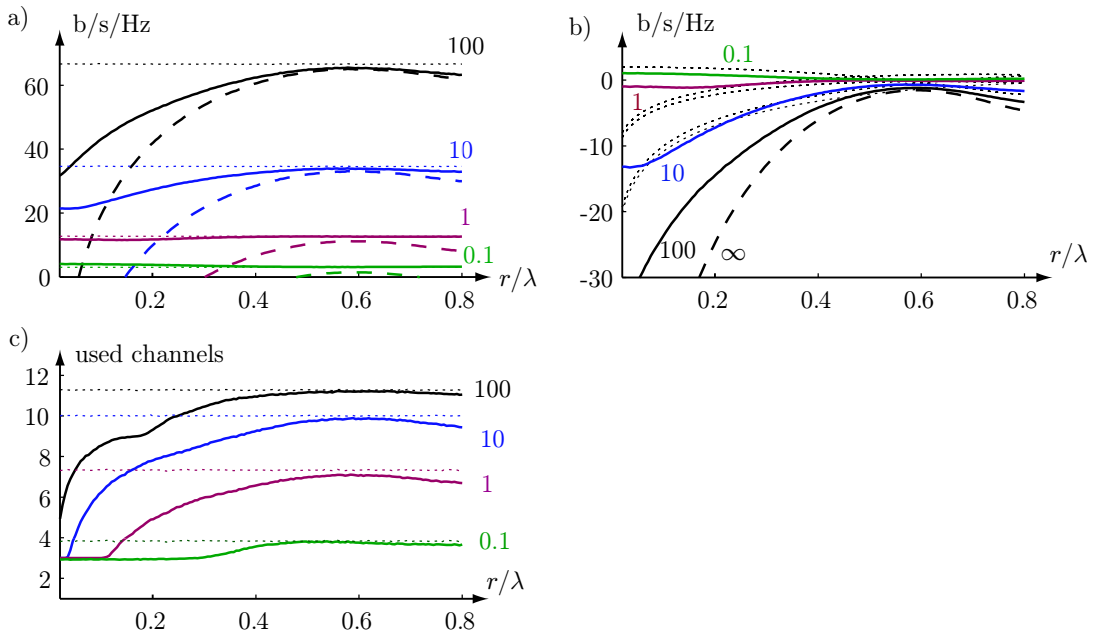

Figure 5: Properties of the MIMO cube as a function of the antenna radius for SNR values of $100, 10, 1$, and 0.1. a) The ergodic capacity. The solid and dotted lines show the ergodic capacity using (3.2) for the MIMO cube, $\overline{C}_{\mathbf{\Sigma}}$, and the uncorrelated case, $\overline{C}_{\mathbf{I}}$, respectively. The dashed lines show the ergodic capacity in the high SNR approximation, $\overline{C}_{\mathbf{I}} + \Delta C$, using (3.4). b) The solid lines show the correlation loss, (3.3), for the SNR values above. The dashed line shows the high SNR case (3.4). The channel gain from Fig. 2b are shown in $\log_2$ scale by the dotted lines. c) Comparison between the average number of used channels of the MIMO cube case (solid lines) and the uncorrelated case (dotted lines).

[2] G. Arfken. *Mathematical Methods for Physicists*. Academic Press, Orlando, third edition, 1985.

[3] A. Boström, G. Kristensson, and S. Ström. Transformation properties of plane, spherical and cylindrical scalar and vector wave functions. In V. V. Varadan, A. Lakhtakia, and V. K. Varadan, editors, *Field Representations and Introduction to Scattering*, Acoustic, Electromagnetic and Elastic Wave Scattering, chapter 4, pages 165–210. Elsevier Science Publishers, Amsterdam, 1991.

[4] R. T. Compton. The tripole antenna: An adaptive array with full polarization flexibility. *IEEE Trans. Antennas Propagat.*, **29**(6), 944–952, November 1981.

[5] P. F. Driessen and G. J. Foschini. On the capacity formula for multiple input-multiple output wireless channels: A geometric interpretation. *IEEE Trans. on Communication*, **47**(2), 173–176, February 1999.

[6] B. N. Getu and J. B. Andersen. The MIMO cube - a compact MIMO antenna. *IEEE Trans. Wireless Communications*, **4**(3), 1136–1141, 2005.

[7] M. Gustafsson and S. Nordebo. On the spectral efficiency of a sphere. Technical Report LUTEDX/(TEAT-7127)/1–24/(2004), Lund Institute of Technology, Department of Electroscience, P.O. Box 118, S-211 00 Lund, Sweden, 2004. `http://www.es.lth.se/teorel`.

[8] J. E. Hansen, editor. *Spherical Near-Field Antenna Measurements*. Number 26 in IEE electromagnetic waves series. Peter Peregrinus Ltd., Stevenage, UK, 1988. ISBN: 0-86341-110-X.

[9] R. C. Hansen. Fundamental limitations in antennas. *Proc. IEEE*, **69**(2), 170–182, 1981.

[10] R. F. Harrington. *Time Harmonic Electromagnetic Fields*. McGraw-Hill, New York, 1961.

[11] J. D. Jackson. *Classical Electrodynamics*. John Wiley & Sons, New York, second edition, 1975.

[12] W. C. Jakes and D. Cox. *Microwave Mobile Communications*. IEEE Press, 1994.

[13] M. A. Jensen and J. W. Wallace. A review of antennas and propagation for MIMO wireless communications. *IEEE Trans. Antennas Propagat.*, **52**(11), 2810–2854, November 2004.

[14] K. S. Miller. *Complex Stochastic Processes*. Addison–Wesley Publishing Company, Inc., 1974.

[15] A. Paulraj, R. Nabar, and D. Gore. *Introduction to Space-Time Wireless Communications*. Cambridge University Press, Cambridge, U.K., 2003.

[16] J. G. Proakis. *Digital Communications*. McGraw-Hill, third edition, 1995.

[17] T. Svantesson. Correlations and channel capacity of MIMO systems employing multimode antennas. *IEEE Trans. Vehicular Technol.*, **51**(6), 1304–1312, 2002.

[18] R. Vaughan and J. Bach Andersen. *Channels, Propagation and Antennas for Mobile Communications*. Institution of Electrical Engineers, 2003.